Special Section: COVID-19 Pandemic

Vol. 4, No. 2 (2020)
ISSN: 2532-5876

DOI: 10.13133/2532-5876/17224

# The Role of Airflow in Airborne Transmission of COVID-19

*Rodolfo Guzzi*[a]* & *Leopoldo Stefanutti*[b]*

[a] *Emeritus, Optical Society of America OSA*

[b] *Former director of the Geophysica-EEIG, Director of the Sundrone Project*

***Corresponding authors:** Rodolfo Guzzi, Email rodolfoguzzi2@gmail.com; Leopoldo Stefanutti, Email l.stefanutti@sundroneproject.com

**Abstract**

The spreading of virus via air pathway has been investigated with simple examples using the Navier–Stokes equations and their application with uncompressible flow and in presence of convection due to heat transfer. Given the results, we argue that the minimum spacing for safety between persons depends on the ratio between the height and length of an artifact, here shown as a cavity box. We found that the best spacing among people is obtained when the ratio is 1:5. This means that the safety consists in staying as far away as possible or using mask properly. In case of confluence between street and square, the Navier–Stokes equations exhibit turbulence at the edges of the system.

**Keywords:** aerosol, flow, COVID-19, droplets.

**Citation:** Guzzi R & Stefanutti L 2020, "The role of airflow in airborne transmission of COVID-19", *Organisms: Journal of Biological Sciences*, vol. 4, no. 2, pp. 121-131. DOI: 10.13133/2532-5876/17224.

## Introduction

In a recent paper, Zhang *et al.* (2020) explain the contribution of airborne transmission on Covid-19. They consider dominant the role of aerial transmission and state that airborne transmission may have played a role in pathogenic avian influenza.

Their experimental and observational studies on interhuman transmission seem to indicate a significant role of aerosols in the transmission of many respiratory viruses, including influenza virus, SARS-CoV-1, and Middle East Respiratory Syndrome coronavirus (MERS-CoV). For example, airborne coronavirus MERS-CoV exhibited strong capability of surviving, with about 64% of microorganisms remaining infectious 60 min after atomization at 25 °C and 79% relative humidity (RH). On the other hand, rapid virus decay occurred, with only 5% survival over a 60-min procedure at 38 °C and 24% RH, indicative of inactivation. Recent experimental studies have examined the stability of SARS-CoV-2, showing that the virus remains infectious in aerosols for hours (see Van Dorelman, 2020) and on surfaces up to days (see Chin *et al.* 2020). They based their argument on the measurements done in Wuhan hospitals and outdoor in northern Italy. Of course, the concentration of virus is accumulated in close environment and diluted in open air. Removal of virus bearing particles by deposition is size dependent; residence time in air is closely associated to air mixing. The lifetime of droplets injected in air from infected persons is subjected to complex mechanisms. First of all, in absence of turbulence larger particles > 5 microns are settled out in short range and contaminate surface, object and persons while atomized particles < 5 microns are dispersed in

air. The lifetime depends on various factors mainly the presence of high humidity and temperature. The wind velocity may dry the droplets. In principle the atomized droplets, arising from coughing and sneezing, interact with dry or wet aerosol present in air and can be dispersed in a longer range due to flow of air. Binbin Wang *et al.* (2020) made a model of the transport and fate of human expiratory droplets using different approaches and applying different particle models for the free fall of droplets. They explored continuous and impulse cough jet to turbulent fluctuations. Their results presented a model to understand the fundamental dynamics of exhaled droplets in human respiratory activities. The model solves the governing equations of droplets and uses a continuous random walk model to simulate turbulent fluctuations in violent expiratory events. The validation of the model shows the improvement in the prediction of dispersion of median-sized droplets. They show that these droplets are sensitive to environmental conditions, including temperature, humidity, and ambient flows. Applying the model to a set of idealized conditions such as free-fall and continuous jets, they demonstrate significantly different impacts of environmental parameters on different size droplets. The interesting point lays in a realistic droplet size distribution and cough duration, quantifying the transport and fate of droplets in the near field of source and the potential influences by ambient conditions. In veterinary medicine, Zhao at al. (2019) have recently confirmed the role of dust transport in viral epidemics spread among farms, such as foot-and-mouth syndrome in cattle and pigs and avian influenza.

Burgio *et al.* (2020) did not consider the hypothesis of airborne transmission to be of primary importance. They assume that at least in this initial phase of the epidemic in Italy, the areas characterized by the highest lethality rates are also the most polluted of the country. Their claim has long been known: atmospheric particulate matter (droplets) is an effective vector for the transport of viruses and for the spread of viral infections. During the avian flu outbreaks, it was even shown that the particulates had carried the fearsome H5N1 for long distances and that there was an exponential correlation between the quantities of cases of infection and the concentrations of PM10 and PM2.5. Even though correlation between the presence of viruses in the particulate matter and epidemic outbreaks has never yet been proved, there is increasingly evidence that most of the infections occur through human contact and in closed and crowded environments (families, public places, and unfortunately hospitals and healthcare residences). Minimal quantities of viruses transported by the particulates do not seem to play a significant role in this context.

As Zhang *et al.* (2020) observed, the pattern of contagiousness in Wuhan, Italy, New York City, and all the United States had different fate. According to their analysis, contagiousness in Italy and New York City started dropping not when the lockdown was issued, but only after a massive use of face masks was imposed (see Figure 1). From the same figure one may see that Italy's lockdown started on March 9th, but only on April 6th the use of face masks became compulsory. The interval between these two dates is of about 4 weeks, while the incubation time of SARS-COV-2 is of about two weeks. In Italy (Figure 1 in the middle), the lockdown was issued on April 6, but only after April 20 the number of new infections started to decrease. A similar pattern was observable in New York City. In Wuhan, after the strict lockdown the number of new cases remained constant (see Liu *et al.*, 2020).

The interval between the previous dates is of about 4 weeks, while the incubation time of SARS-COV-2 is of about two weeks. During these 4 weeks, no reduction in the number of new infected people was measured, and most of the new infected, often in critical conditions, were hospitalized in intensive care departments. Curve B and C indicate, relatively for Italy and New York City, the reduction of contagiousness after April 6 in Italy and April 20 in New York City, while in the rest of the United States the contagious continued to grow, as shown in Figures 2 and 3.

We have drawn in Figure 4 and Figure 5a,b, similar curves for Italy during the same period. It is evident that the policy of social distancing and face masks had a tremendous differentiating effect between Italy and the USA, where a policy of lockdown, social distancing, and face masks were adopted in a chaotic way and reopening was often decided while the infection was growing.

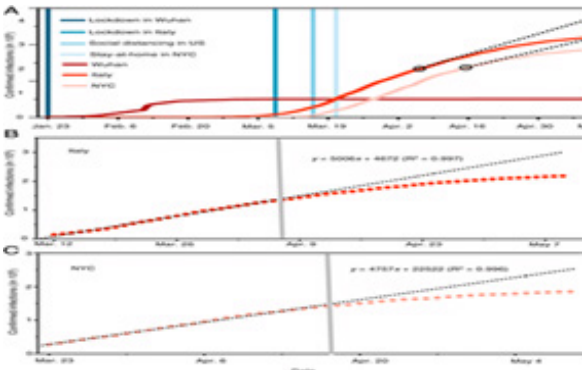

**Figure 1:** All three figures show the evolution of the infections in Wuhan, Italy, and New York City. Source: Zhang et al. (2020).

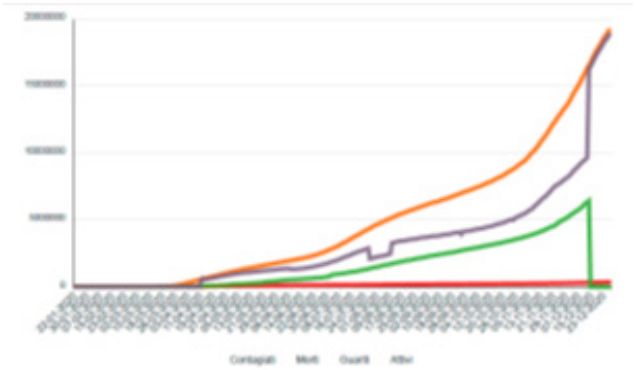

**Figure 2:** Coronavirus in USA from March 18, to December 23, 2020. Yellow: affected. Green: recovered. Black: active ill. Red: dead. Source: https://statistichecoronavirus.it/.

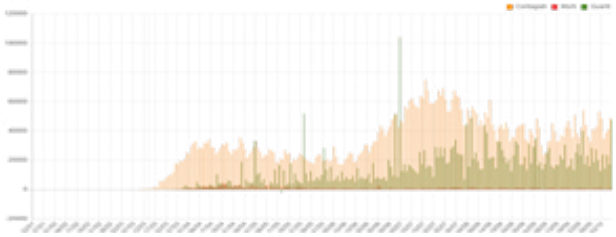

**Figure 3:** The U.S. new cases from March 2020 to today. Brown: contagious. Green: recovered. Dark brown: dead. Source: https://statistichecoronavirus.it/.

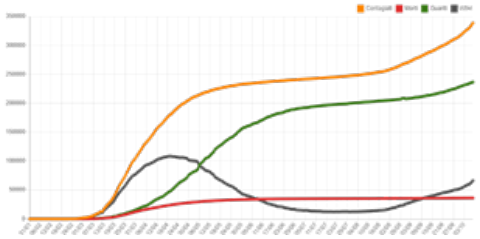

**Figure 4:** Covid 19 cases in Italy. Yellow: affected. Green: recovered. Black: active ill. Red: dead. Since April the curve grows very slowly up to the end of August, but the curve representing the dead remains flat. Source: https://statistichecoronavirus.it/.

In order to understand the virus spread dynamics, this paper analyzes the flow modes of air in selected case studies from which we can derive the dispersion of droplets. By our numerical experiment, based on a simulation, we explored the flow dispersion both inside a street canyon and in a close site where the combined effect of flow and temperature play an important role.

## 1. Modelling the flows

In order to improve the prediction of spreading of median-sized droplets, which are sensitive to the environment and critical to the decision of public health we need to model the flow in different situations.

Viruses are acellular organisms of sub-microscopic dimensions of the order of 60-120 nm. For lacking autonomous metabolism, they are parasites and replicate inside cells of other organisms. By coughing, but also by just breathing, we emit micro droplets of the order of the micron. The virus may travel on such droplets. In the absence of wind such droplets reach rapidly the floor or are dispersed in air, and their concentration per unit volume rapidly decreases. In the presence of strong droplets concentration, as in the case of fog or relevant atmospheric pollution, the high concentration of infected droplets could remain in air for a longer period. It is important to know the survival conditions of the virus (humidity, temperature, and pressure). Only this way it is possible to establish for how long and in which conditions the virus can remain dangerous in air. Probably the virus diffusion on the big cruise ships occurred via the air conditioning pipes, fresh air, and relatively high humidity. Such investigation is not simple and rapid. Aerosols can travel for thousands of kilometres, at different altitudes. As an example, we may recall that there are polluting clouds travelling at heights above 5000 m from South East Asia to Europe. We do not believe that such clouds can transport the virus, but to tackle such a complex problem it would be important

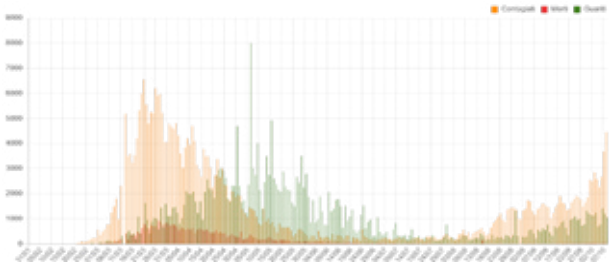

**Figure 5a:** Daily new cases in Italy since April 2020. Brown: contagious. Green: recovered. Dark brown: dead. Source: https://statistichecoronavirus.it/.

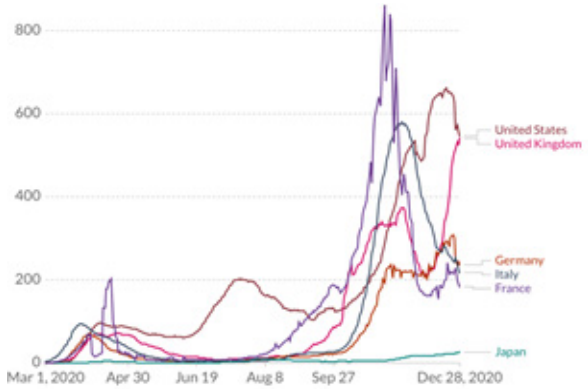


**Figure 5b:** Confirmed positive cases per million of inhabitants. Rolling 7-average. This picture shows the difference in health policies in several European countries, the U.K., U.S.A., and Japan. Source: https://ourworldindata.org/coronavirus/.

the study of the virus inside a climatic chamber, where temperature, pressure, humidity, aerosol concentration, etc. could be varied. It is also crucial to understand the difference between aerosol and droplets. Even though the droplets need a hygroscopic nucleus to grow, aerosol is the solid part embedded in air (air plus solid). Droplets are due to condensation of water vapor before the saturation in presence of condensation nuclei. We, hence, believe that it is fundamental to determine the time during which the concentration of virus remains high in air. This depends both from the survival time in air of the virus and by the possibility, when survival time is not negligible (order of seconds), that the concentration of the virus remains high, even in the presence of a mild wind and is transported in high concentration. We assume that this may occur when the airflow remains laminar. In a closed environment, the air does not move or moves slowly, and its movement may be due to air conditioning systems. In any way, we can assume, as it probably happened in the ducts transporting the air conditioned from one cabin to the other in the great cruising ships that the air speed is always below one $msec^{-1}$.

In a closed environment, if the air motion is laminar, as in figure 6a, it is possible that a high virus concentration remains in the environment.

The passage from laminar to turbulent flow is ruled by the Reynolds number:

$$\mathrm{Re} = \frac{uL}{\nu} = \frac{\rho u L}{\mu}$$

Where u, is the air velocity, v is the air density, equal to 1,23 $Kgm^{-3}$; μ is its viscosity equal to 0,0185, mPa at 25°C, and L indicates the width of a pipe or similar. The passage from laminar to turbulent flow occurs in region of Re of the order of 2000.

In a closed environment, all virus transmission systems may operate simultaneously (direct contact, deposition, and aerial transport). Outside, the situation may be different.

As first numerical experiment, we have simulated the condition occurring in one of the streets of our ancient cities: narrow and with not very high buildings. We have considered the simplest case: an open box, simulating a street, with different ratios between the height of the buildings and the width of the street, i.e. 1:2, 1:3, and 1:5.

Figure 7 presents the most general cavity open at the top where the top lid can slide horizontally. When the top lid is not moving, the internal air (or fluid) is stationary. However, when the lid starts moving it makes the fluid circulate inside the cavity. This can resemble a street canyon where the lateral walls of box are buildings, and the bottom of the box represents the surface of the street. The top lid movement simulates the windy condition. Appendix 1 shows the detail of the model and the CFD techniques we used.

As the computing time is very long and complex, we have carried out, more systematically, a 2D simulation of the airflow in a cross section of the street, as shown in the following figures.

The wind at the top of the building is assumed equal to 1 m $sec^{-1}$. At the ground and on the sides of the buildings the wind is equal to 0 $msec^{-1}$. The result for Re =100 is reported in figure 8. The ratio between height and length is 1:1. We use the 2D Navier–Stokes equations with constant temperature. The other parameters are shown in Figure 7.

The variation of the Reynolds number between 100 and 2500 did not change the figure but in squeezing the two lobes and producing a very small lobe at the bottom left with no influence on the middle-high flow.

Figure 8 allows us to observe two mega cells, a larger one in the upper side, and a smaller one in the lower part. Substantially, the air flux remains laminar in the two cells. This means that viruses emitted by a person standing on the left side of the street, near the wall, can reach the opposite side keeping the same concentration. Hence, if the concentration is high enough, a breathing person on the other side of the street will inhale a high concentration of viruses.

Further, by keeping Re=100 we changed the ratio between the height of the buildings and the width of the street to 1:2, 1:3, 1:4, and 1:5. We plotted the results respectively in Figure 9 (left and right) and Figure 10 (left and right).

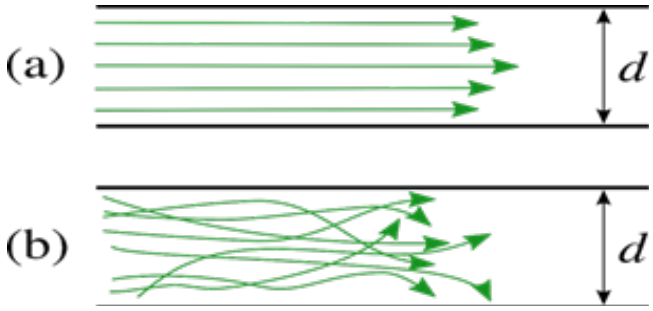


**Figure 6:** Laminar (a) and turbulent air flow (b).

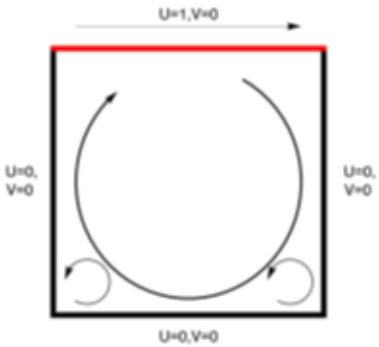


**Figure 7:** Cross section of the simulated street, u and v indicate the wind velocity in the horizontal and vertical direction.

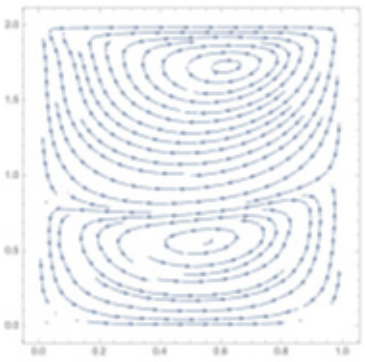

**Figure 8:** Air flow in the street cross section, computation for Re=100 and u at the top of the street equal 1 m/sec.

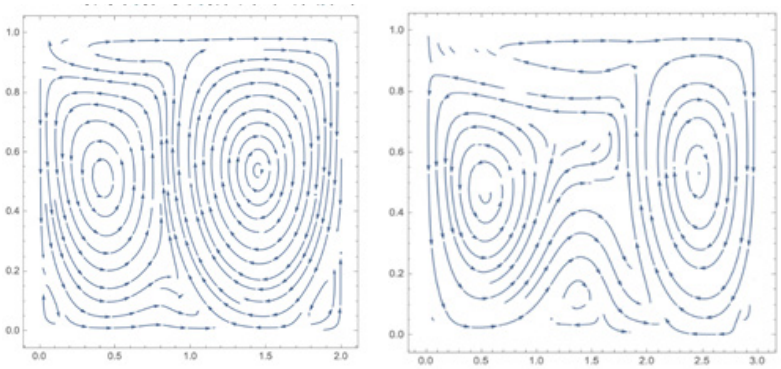

**Figure 9:** Flow for Re= 100 where the ratio between high and length is 1:2 (left); Re=100 with ratio between High and Length 1:3 (right).

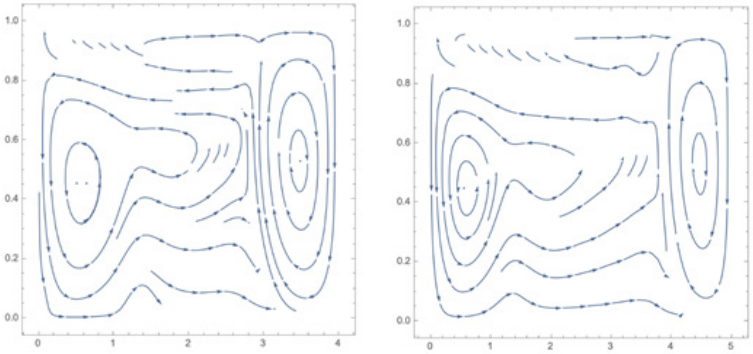

**Figure 10:** 1:4 height and length ratio (left) and 1:5 height and length ratio (right).

The system of flow shows two interacting lobes. This indicates that the ratio between height and width is a critical parameter. It is then apparent that the behaviour of the airflow depends strongly on the ratio between height of the buildings and the width of the street. As this ratio increases, i.e., as the street becomes larger than the height, the system of flow produces non-interacting lobes.

Since the virus lifetime strongly depends on temperature and humidity and may decay more rapidly in the case of high Relative Humidity, we introduce the effect of temperature along the walls (see Figure 11). Here, the system exhibits different patterns. The cavity is closed and he ratio between the height and the base is 1:1.

We have used the most general 2D Navier–Stokes with heat transfer incorporating the Boussinesq approximation (see Appendix 1) coupled with thermal convection diffusion equation. In this model, where the flow is governed by the continuity equation, the equation of motion and the energy equation under Boussinesq hypothesis is given in Appendix 1.

As result we obtain the figures 12a,b, where the ratio between height and the base is 1:2.

Figures 12a and 12b show the existence of one cell; the flow seems even more regular and horizontal for most of the area of the cross section, with a sharper ascent (warm side) and descent (cold side) along the walls.

In our simulation we use the Rayleigh Number equal to 100000. In Figure 12a we show the temperature pattern and in figure 12b the air flow in case of ratio 1:2.

The same experiment done with the ratio between height and base is 1:5 as shown in Figure 13.

In this case, the temperature difference has caused the air flux to become much more regular than in the case of Figure 9 (right), where the same ratio 1:5 has been assumed but no temperature difference between the two different walls had been assumed. In the previous case, two non-interacting lobes occurred. In this case, the circulation is extremely regular from one side to the other of the walls. It is interesting to note the effect of the temperature when the hottest and the coldest fluid mix, as can be seen in the sequence of Figure 14. In this case, the ratio between walls height and base length is 1:2, with the number of Prandtl Pr = 0.71 and the number of Rayleigh $Ra=10^5$.

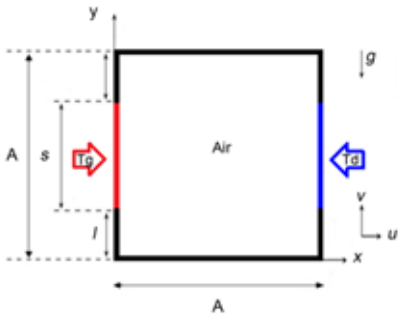


**Figure 11:** One side of the street is illuminated by the sun, the other side is in the shade. Source: Kane et al. (2017).

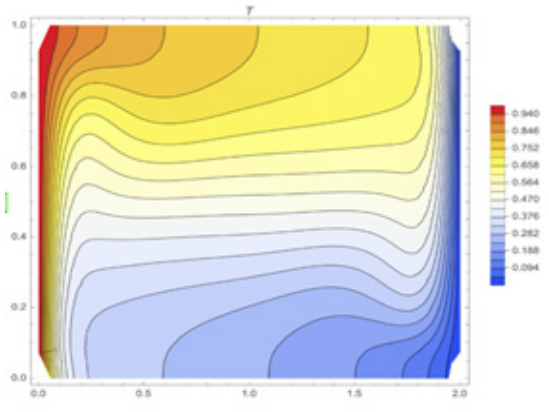

**Figure 12a:** Temperature pattern.

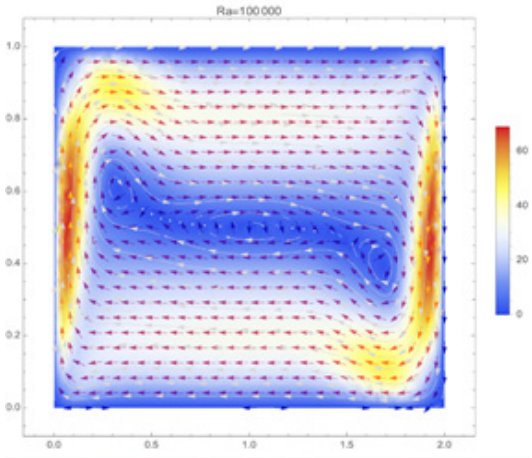


**Figure 12b:** Corresponding air flow.

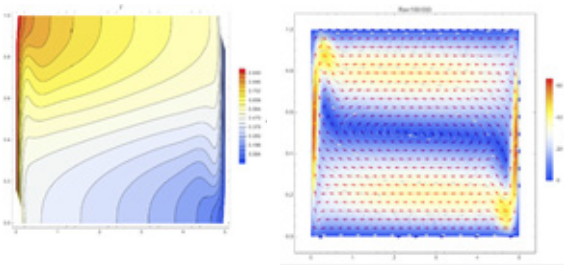

**Figure 13:** Same as figure 12a,b but with a ratio 1:5.

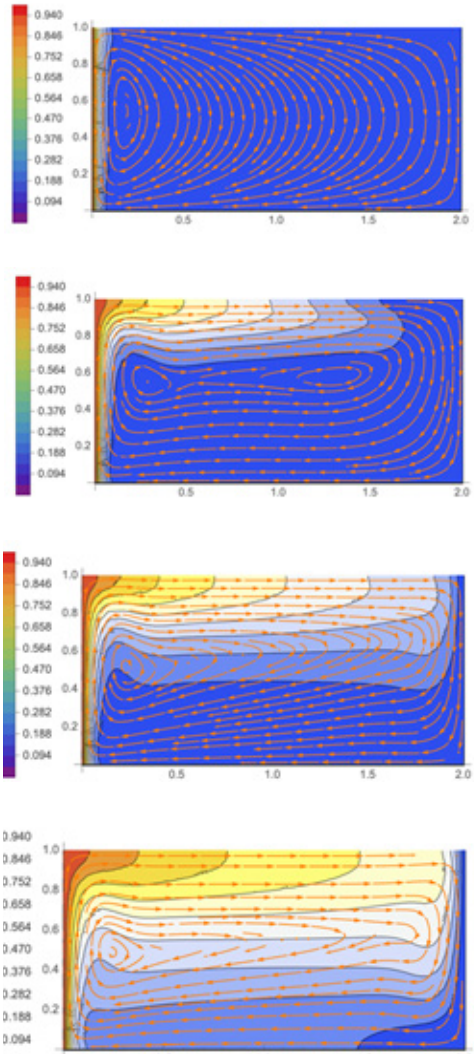

**Figure 14:** Sequence of mixing fluid in presence of a temperature gradient. From the first to the last picture the system shows the flow following the distribution of temperature. The computation has been performed at steps of 30 sec. The gradient between the "hot" and the "cold" walls is of some degree (the gradient is contained into Rayleigh number).

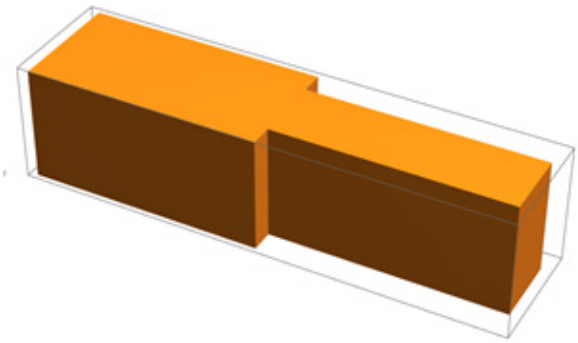

**Figure 15:** Example of 3D representation for simulating the confluence of a street in a square.

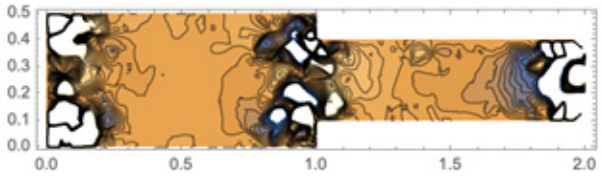

**Figure 16:** Half-height horizontal cross section of a square-street confluence. In case of edges, the Navier–Stokes exhibit turbulence.

In order to understand more about the effect of a 3D flow in absence of temperature effect, we have also simulated the case of a square and a street, assuming the square to be as in figure 15.

To better understand the effect of the edges we sliced the 3D object in different layers. The results of one of them is given in Figure 16.

At the edges, we note a strong concentration of air turbulence and an increase of airflow velocity due to Venturi effect. This might cause locally a strong additional concentration of viruses even if the flow is now turbulent.

## Conclusions

Our simulations evidence that in order to avoid the transport of infected droplets, a several-meter distance, depending on the ratio between the boundaries, is required.

The Reynolds number shows that the circulation remains laminar in a street whose width is up to 10 meters when the wind velocity at the top of the buildings is equal to 4 msec$^{-1}$. Only when we consider locations larger than 100 m, then the circulation appears to be always turbulent. The distance to avoid completely the contagion is of the order of 50 meters.

In case of heat convection, in the presence of high Relative Humidity the droplets' lifetime could be of the order of 1 min, while in the case of low humidity it can reach values up to 8 minutes before settling. If we consider an air velocity of 1 m sec$^{-1}$, then the parcel may travel 60 meters in 1 minute and 480 meter in 8 minutes. The presence of heat flow influences the spreading of particles. The flow changes in a few minutes and its pattern mixes the warm and cold air that transports the particles to a further distance.

In this paper, the spreading of virus for air pathway has been investigated with simple examples using the Navier–Stokes equations and their application with uncompressible flow and in presence of heat transfer convection. Given the results, we argue that the minimum safe spacing between people depends on the ratio between the height and length of an artefact, here proposed as a cavity box. We found that the best spacing among people is achieved when the ratio is 1:5. This means that it is safe to stay as far away as possible or properly use mask. A 3D model applied to a more complex structure, such as a street-square confluence. The NS equations exhibit turbulence at the edges of the system.

## Appendix 1

The main ruling differential equation of fluid flow and heat transfer is given through the Navier-Stokes (N-S) equations, which are are based on the conservation of mass, linear momentum (Newton second law), and energy (first law of thermodynamics). Due to different mathematical characters of governing equations for compressible and incompressible flow, the Computational Fluid Dynamics CFD codes are usually written for only one of them. For compressible flow simulation, it is usual to drop the viscous terms obtaining the Euler's equation. This is of common use for obtaining the pressure distribution around a flying body, where the viscous effects are squeezed inside e very thin boundary layer. On the other hand, uncompressible flows have a known constant value. In this paper we use an incompressible flow approach that is valid for any coordinate system.

In fluid dynamics, the Reynolds number, $\mathrm{Re}=\rho UL/\mu$, corresponds to the ratio of inertial forces to viscous forces. It measures how turbulent the flow is, where low Reynolds number flows are laminar and high Reynolds number flows are turbulent.

The Mach number, $\mathrm{M}=U/c$, corresponds to the ratio of the fluid velocity, $U$, to the speed of sound in that fluid, $c$ and measures flow compressibility.

In Cartesian flows we have the following equations:

$$\frac{\partial u}{\partial x}+\frac{\partial v}{\partial y}+\frac{\partial w}{\partial z}=0$$

$$\frac{\partial u}{\partial t}+u\frac{\partial u}{\partial x}+v\frac{\partial u}{\partial y}+w\frac{\partial u}{\partial z}=-\frac{1}{\rho}\frac{\partial p}{\partial x}+v\left(\frac{\partial^2 u}{\partial x^2}+\frac{\partial^2 u}{\partial y^2}+\frac{\partial^2 u}{\partial z^2}\right)+f_x$$

$$\frac{\partial v}{\partial t}+u\frac{\partial v}{\partial x}+v\frac{\partial v}{\partial y}+w\frac{\partial v}{\partial z}=-\frac{1}{\rho}\frac{\partial p}{\partial y}+v\left(\frac{\partial^2 v}{\partial x^2}+\frac{\partial^2 v}{\partial y^2}+\frac{\partial^2 v}{\partial z^2}\right)+f_y$$

$$\frac{\partial w}{\partial t}+u\frac{\partial w}{\partial x}+v\frac{\partial w}{\partial y}+w\frac{\partial w}{\partial z}=-\frac{1}{\rho}\frac{\partial p}{\partial z}+v\left(\frac{\partial^2 w}{\partial x^2}+\frac{\partial^2 w}{\partial y^2}+\frac{\partial^2 w}{\partial z^2}\right)+f_z$$

$$\rho c_p\left(\frac{\partial T}{\partial t}+u\frac{\partial T}{\partial x}+v\frac{\partial T}{\partial y}+w\frac{\partial T}{\partial z}\right)=k\left(\frac{\partial^2 T}{\partial x^2}+\frac{\partial^2 T}{\partial y^2}+\frac{\partial^2 T}{\partial z^2}\right)+\phi$$

Where v is the viscosity, p is the pressure, T is the temperature, $\rho$ is the density, $c_p$ is the specific heat, u, v and w are the flow components related to the coordinates x, y, z. and $k$ is the thermal conductivity.

$$\phi=\mu\left\{2\left[\left(\frac{\partial u}{\partial x}\right)^2+\left(\frac{\partial v}{\partial y}\right)^2+\left(\frac{\partial w}{\partial z}\right)^2\right]+\left(\frac{\partial v}{\partial x}+\frac{\partial u}{\partial y}\right)^2+\left(\frac{\partial w}{\partial y}+\frac{\partial v}{\partial z}\right)^2+\left(\frac{\partial u}{\partial z}+\frac{\partial w}{\partial x}\right)^2\right\}$$

The dissipation function is given by

The previous equations represent the conservation of mass (the first one), the conservation of linear momentum (the next three) and the conservation of energy for incompressible flows (the last).

In order to simplify the system for computation, it is preferable to write the governing equations in nondimensional form, selecting characteristic quantities that describe the flow problem. These are the characteristic length L of a flow, its velocity $U_c$, pressure $p_c$, and temperature $T_c$, $f_x$, $f_y$, $f_z$ are the external forces applied to the fluid that in our case are zero.

Then the following nondimensional parameters can be defined:

$$t^* = \frac{t}{L/U_c}, x^* = \frac{x}{L}, y^* = \frac{y}{L}, z^* = \frac{z}{L}, u^* = \frac{u}{U_c}, c^* = \frac{v}{U_c}, w^* = \frac{w}{U_c}, \ldots$$
$$\ldots, p^* = \frac{p - p_c}{\rho U_\xi^2}, T^* = \frac{T - T_c}{\Delta T}$$

Where $\Delta T$ is a known reference temperature difference in the flow field between a constant wall temperature and $T_c$. Using the characteristic quantities, previous equations can be converted as:

$$\frac{\partial u^*}{\partial x^*} + \frac{\partial v^*}{\partial y^*} + \frac{\partial w^*}{\partial z} = 0$$
$$\frac{\partial u^*}{\partial t^*} + u^*\frac{\partial u^*}{\partial x^*} + v^*\frac{\partial u^*}{\partial y^*} + w^*\frac{\partial u^*}{\partial z^*} = \frac{\partial p^*}{\partial x^*} + \frac{1}{Re}\left(\frac{\partial^2 u^*}{\partial x^{*2}} + \frac{\partial^2 u^*}{\partial y^{*2}} + \frac{\partial^2 u^*}{\partial z^{*2}}\right)$$
$$\frac{\partial v^*}{\partial t^*} + u^*\frac{\partial v^*}{\partial x^*} + v^*\frac{\partial v^*}{\partial y^*} + w^*\frac{\partial v^*}{\partial z^*} = \frac{\partial p^*}{\partial y^*} + \frac{1}{Re}\left(\frac{\partial^2 v^*}{\partial x^{*2}} + \frac{\partial^2 v^*}{\partial y^{*2}} + \frac{\partial^2 v^*}{\partial z^{*2}}\right)$$
$$\frac{\partial w^*}{\partial t^*} + u^*\frac{\partial w^*}{\partial x^*} + v^*\frac{\partial w}{\partial y^*} + w^*\frac{\partial w^*}{\partial z^*} = \frac{\partial p^*}{\partial z^*} + \frac{1}{Re}\left(\frac{\partial^2 w^*}{\partial x^{*2}} + \frac{\partial^2 w^*}{\partial y^{*2}} + \frac{\partial^2 w^*}{\partial z^{*2}}\right)$$
$$\frac{\partial T^*}{\partial t^*} + u^*\frac{\partial T^*}{\partial x^*} + v^*\frac{\partial T^*}{\partial y^*} + w^*\frac{\partial T^*}{\partial z^*} = \frac{1}{\mathrm{RePr}}\left(\frac{\partial^2 T^*}{\partial x^{*2}} + \frac{\partial^2 T^*}{\partial y^{*2}} + \frac{\partial^2 T^*}{\partial z^{*2}}\right) + \frac{Ec}{Re}\phi^*$$

The following quantities have been introduced: the Reynolds number (Re= $U_c L/ \upsilon$) in the momentum and energy equations, the Eckert number ($Ec=U_c^2/(c_p \Delta T)$ which is the ratio of flow's kinetic energy to a representative enthalpy difference, the Prandtl number ($Pr=\upsilon/\alpha=\upsilon/(k/\rho c_p)$) which is the ratio of momentum and thermal diffusivities. In case of incompressible viscous flow, it is usual to introduce the Reynolds number Re=100, 1000.

Solving the above system in general is difficult but a simple experiment can imitate some common environmental dynamics.

After selecting the geometry, it is necessary to define the dynamic boundary and thermal conditions. Since there are not known analytical solutions, the only choice is to obtain a solution using numerical methods by the treatment of the derivatives.

Here is the algorithm we have followed.

i) Take the domain and discretize it, that means the solution *u(x,y,z)*, v(x,y,z), w(x,y,z) are computed at discrete points $x_i$, y, z defining a set of grid.

ii) The derivatives are expressed as some linear combination of *u(x,y,z)*, v(x,y,z), w(x,y,z)

iii) The final system is changed from a system of differential equations to a system of algebraic equations for *u(x,y,z)*, v(x,y,z), w(x,y,z), solved using one of many root finding algorithms.

Following the algorithm outlined above, the first step is to define the domain. This means that we have to define the geometry, for instance a cavity, open or not, depending if we are making some numerical experiment in a room or in a canyon street. The second step is to find an approximation to the derivatives that are approximated as:

$$\frac{\partial u}{\partial x}(x_i, y_i, z_i) \approx \sum a_{ij} u(x_j, y_j, z_i)$$

This form of approximation is called finite difference approximation. The coefficients can be computed using the traditional Taylor series.

We use the Dirichlet boundary conditions that are the values that a solution needs to take along the boundary of the domain and take into account its shape. In order to simulate the flow we divided the area given from Figure 7 with 100 points (see figure A1). At each of these grid points, the velocities and pressure have to be computed.

In figure A1 we present the most general cavity open at the top where the top lid can slide horizontally. When the top lid does not move, the internal air (or fluid) is stationary. However, when the lid starts moving, the motion of the lid makes the fluid circulate inside the cavity. This can resemble a street canyon where the lateral box walls represent buildings and the box bottom

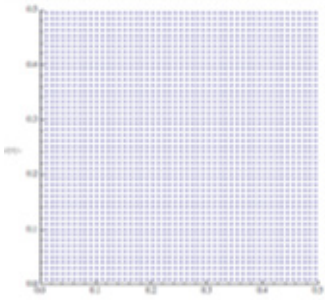

**Figure A1:** The area of figure 7 with 100 points.

represents the street surface. For the flow in this cavity, the Navier–Stokes equations can be simplified. Let us assume that the flow does not change in function of time, that it does not change in the z direction, and that the temperature remains constant. This simplifies our equations to:

Equation 1A

$$\frac{\partial u^*}{\partial x^*} + \frac{\partial v^*}{\partial y^*} = 0$$

$$u^* \frac{\partial u^*}{\partial x^*} + v^* \frac{\partial u^*}{\partial y^*} = \frac{\partial p^*}{\partial x^*} + \frac{1}{Re}\left(\frac{\partial^2 u^*}{\partial x^{*2}} + \frac{\partial^2 u^*}{\partial y^{*2}}\right)$$

$$u^* \frac{\partial v^*}{\partial x^*} + v^* \frac{\partial v^*}{\partial y^*} = \frac{\partial p^*}{\partial y^*} + \frac{1}{Re}\left(\frac{\partial^2 v^*}{\partial x^{*2}} + \frac{\partial^2 v^*}{\partial y^{*2}}\right)$$

The top lid drags the fluid below it, which generates a swirling motion. This initial swirling motion produces in turn its own swirling motion —a big gear turning smaller gears. A cross-section of the u, v indicates the wind velocity in the horizontal and vertical direction. The wind at the top of the building is assumed equal to 1 $msec^{-1}$. At the ground and on the sides of the buildings the wind is equal to 0 $msec^{-1}$.

The cavity can be made as larger or as smaller as we desire. In the second case top, the lid can be moved fast or slow simply by changing the Reynolds number. We varied the Reynolds number between 100 and 2000. This number can also be used to describe whether the fluid inside the box is water, air, or any other substance of choice. When the fluid of particles flows without intersecting the paths of each other and the velocity of the particles is always tangential to the path of the particle, the flow is said to be streamline. When the streamline flow occurs, the layers of fluid particles tend to slide over the adjacent particle without disturbing the motion of others, and this occurs in layers or laminas of fluid flow. Such a flow is known as a laminar flow. Laminar flow or streamline flow occurs when the fluid velocity is relatively low. In laminar flow, the layer in contact with a stationary surface has zero velocity and, in the direction perpendicular to the surface, the velocity of the layers tends to increase. Also, the velocity, pressure, density, and other fluid dynamic properties remain unchanged at every point in the space of the flow. Reynolds number indicates how well a fluid may undergo laminar flow. When the Reynolds number is low, the flow tends to be laminar, and the viscous forces are the dominant form of interaction between the layers. When the Reynolds number is high, the flow tends to be turbulent, and inertial forces are the dominant form of interaction between the layers.

When the fluid properties in a flow vary rapidly with time, i.e., when the changes in the velocity, pressure, density, and other flow properties show random and arbitrary changes, the flow is known as a turbulent flow. The fluid flow within a uniform cylindrical pipe with a finite length, also known as a Poiseuille flow, will have turbulence in the flow when the Reynolds number reaches the critical number, around 2040. However, generally, the flow may not explicitly be turbulent when the Reynolds number is more than 10000.

Eddies, cross currents and vortices are typical of any turbulent flow.

• Laminar flows feature low velocities and low Reynolds number, while turbulence flows show high velocities and high Reynolds number.

• Laminar flows feature a regular and streamline path of the fluid lines, no lateral disturbance, and layers. Turbulent flows have irregular and chaotic patterns.

• Laminar flows are constant at a point in space, where turbulent flows are stochastic.

In case of a room one can choose a cavity differentially heated, formed by two vertical walls as reported in figure 11. In this case of natural convection, we use a second model given by the equation 2A. The problem to be considered is that of the two-dimensional flow of a Boussinesq fluid of Prandtl number 0.71 in an upright square cavity of side L. Both velocity components are zero on the boundaries. The horizontal walls are insulated, and the vertical sides are at temperatures Tg and Td. The solution is given by DeVahl Davies (1983). Convection is the transfer of thermal energy due to the motion of fluids. Natural convection is defined as the fluid flow and heat transport arising due to density and temperature differences in the fluid. The chosen geometry is a square cavity differentially heated. It is formed by two vertical walls, each of which is heated at its center. The left active part has a higher temperature (Tr + ΔT/ 2) than that of the right active part (Tr – ΔT /2). The boundary conditions are Dirichlet type.

The flow is governed by the continuity equation, the equations of motion and the energy equation under convection in the Boussinesq hypothesis. $U_r$ =

α/A for velocity, A for length, $A/U_r$ = A2/α for time and θ= (T−Tr)/ΔT corresponds to the dimensionless temperature. Then:

Equation 2A

$$\frac{\partial U}{\partial X}+\frac{\partial V}{\partial Y}=0$$

$$\frac{\partial U}{\partial \tau}+U\frac{\partial U}{\partial X}+V\frac{\partial U}{\partial Y}=-\frac{\partial P}{\partial X}+Pr\left(\frac{\partial^2 U}{\partial X^2}+\frac{\partial^2 U}{\partial Y^2}\right)$$

$$\frac{\partial V}{\partial \tau}+U\frac{\partial V}{\partial X}+V\frac{\partial V}{\partial Y}=-\frac{\partial P}{\partial Y}+Pr\left(\frac{\partial^2 V}{\partial X^2}+\frac{\partial^2 V}{\partial Y^2}\right)+Ra\cdot Pr\cdot\theta$$

$$\frac{\partial \theta}{\partial \tau}+U\frac{\partial \theta}{\partial X}+V\frac{\partial \theta}{\partial Y}=\frac{\partial^2 \theta}{\partial X^2}+\frac{\partial^2 \theta}{\partial Y^2}$$

We have the following boundary conditions (hydrodynamic and thermal) at the walls:

X=0, (Heated part of the left wall), U=V=0, θ=1;

X=1, (Heated part of the right wall), U=V= 0, θ=0;

X=0 and X1, (Adiabatic parts of left and right walls), U=V=0; $\partial\theta/\partial x = 0$;

Y=0 and Y =1 (Lower and upper walls), U=V=0; $\partial\theta/\partial y = 0$.

The dimensionless numbers used is the Prandtl number Pr=v/α, that is physically defined as ratio of momentum diffusivity to thermal diffusivity. It provides a measure of the efficiency of diffusion transport through the velocity boundary layer and the thermal boundary layer. Rayleigh number, Ra, is physically the ratio of buoyancy and viscosity forces multiplied by the ratio of momentum and thermal diffusivities. Below the critical value of the Rayleigh number, heat transfer is primarily due to conduction. Above this critical value, heat transfer is due to convection: $Ra = g\,\beta\Delta T A^3/\nu\alpha$. The numbers for $Ra=10^3,10^4,10^5$. For Pr=0.71 the relation between Ra number and Re is $Re=0.085Ra^{0.455}$ (see Grossmann & Lohse, 2002).

## References


Wang B, Wu H, Wan X-F (2020), "Transport and fate of human expiratory droplets—A modeling approach, *Physics of Fluids*, vol. 32, 083307. Available from: https://doi.org/10.1063/5.0021280

Burgio E *et al.* (2020) COVID-19 (27 Aprile 2020) "Covid-19: The Italian drama", *Epigenetwork* [online] https://www.epigenetwork.it/2020/04/25/covid-19-the-italian-drama/.

Chin A W H *et al.* (2020). "Stability of SARS- CoV-2 in different environmental conditions" *Lancet Microbe*, vol 1, no. 1, E10. Available from: https://www.thelancet.com/journals/lanmic/article/PIIS2666-5247(20)30003-3/fulltext.

De Vahl D G (1983), "Natural Convection of Air in a Square Cavity: A Benchmark Numerical Solution", *International Journal for Numerical Methods in Fluids*, vol. 3, pp. 249–264.

Grossmann S & Lohse D (2002), "Prandtl and Rayleigh number dependence of the Reynolds number in turbulent thermal convection", *Physical Review E*, vol. 66, no. 1, 016305.

Liu Y *et al.* (2020), "Aerodynamic analysis of SARS-CoV-2 in two Wuhan hospitals", Nature, vol. 582, pp. 557 –560. DOI: 10.1038/s41586-020-2271-3.

Kane M K *et al.* (2017), "A study of natural convection of air in a square cavity with partially thermally active side walls", *Open Journal of Fluid Dynamics*, vol. 7, no. 4, pp. 623–641.

Zhang R *et al.* (2020) "Identifying airborne transmission as the dominant route for the spread of COVID-19" *PNAS,* vol. 117, no. 26, pp. 14857-14863. Available from: www.pnas.org/cgi/doi/10.1073/pnas.2009637117.

van Doremalen N, Bushmaker T, & Morris D H (2020), "Aerosol and surface stability of SARS-CoV-2 as compared with SARS-CoV-1", *The New England Journal of Medicine*, vol. 382, pp. 1564–1567. DOI: 10.1056/NEJMc2004973.

Zhao Y *et al.* (2019) "Airborne transmission may have played a role in the spread of 2015 highly pathogenic avian influenza outbreaks in the United States", *Scientific Reports*, vol. 9, 11755. Available from: https://www.nature.com/articles/s41598-019-47788-z#citeas.